energies

MDPI

Article

Rational Design of Electrolyte Additives for Improved Solid Electrolyte Interphase Formation on Graphite Anodes: A Study of 1,3,6-Hexanetrinitrile

Hangning Liu [1], Lin Wang [1], Yi Cao [1], Yingjun Ma [1], Shan Wang [1], Jie Wang [1,2,*] and Haidong Liu [2,*]

[1] College of Chemistry and Pharmaceutical Sciences, Qingdao Agricultural University, Qingdao 266109, China; 20200201033@stu.qau.edu.cn (H.L.); 20212209016@stu.qau.edu.cn (L.W.); caoyi@stu.qau.edu.cn (Y.C.); myj3752@163.com (Y.M.); 20232223023@stu.gau.edu.cn (S.W.)

[2] Department of Chemistry—Ångström Laboratory, Uppsala University, 75121 Uppsala, Sweden

* Correspondence: wangjie@qau.edu.cn (J.W.); haidong.liu@kemi.uu.se (H.L.)

Abstract: The construction of a thin, uniform, and robust solid electrolyte interphase (SEI) film on the surface of active materials is pivotal for enhancing the overall performance of lithium-ion batteries (LiBs). However, conventional electrolytes often fail to achieve the desired SEI characteristics. In this work, we introduced 1,3,6-hexanetrinitrile (HTCN) in the baseline electrolyte (BE) of 1.0 M $LiPF_6$ in Ethylene Carbonate/Dimethyl Carbonate (EC/DMC) (3:7 by volume) with 5 wt.% fluoroethylene carbonate (FEC), denoted as BE-FH. By systematically investigating the influence of FEC: HTCN weight ratios on the electrochemical performance of graphite anodes, we identified an optimal composition (FEC:HTCN = 5:4 by weight, denoted as BE-FH54) that demonstrated greatly improved initial Coulombic efficiency, rate capability, and cycling stability compared with the baseline electrolyte. Deviations from the optimal FEC:HTCN ratio resulted in the formation of either small cracks or excessively thick SEI layers. The enhanced performance of BE-FH54-based LiB is mainly ascribed to the synergistic effect of FEC and HTCN in forming a robust, thin, homogeneous, and ion-conducting SEI. This research highlights the importance of rational electrolyte design in enhancing the electrochemical performance of graphite anodes in LiBs and provides insights into the role of nitrile-based additives in modulating the SEI properties.

Keywords: solid electrolyte interphase; lithium-ion battery; 1,3,6-hexanetrinitrile; graphite electrode; performance

check for updates

Citation: Liu, H.; Wang, L.; Cao, Y.; Ma, Y.; Wang, S.; Wang, J.; Liu, H. Rational Design of Electrolyte Additives for Improved Solid Electrolyte Interphase Formation on Graphite Anodes: A Study of 1,3,6-Hexanetrinitrile. *Energies* **2024**, *17*, 3331. https://doi.org/10.3390/en17133331

Academic Editor: JongHoon Kim

Received: 1 June 2024
Revised: 3 July 2024
Accepted: 4 July 2024
Published: 7 July 2024

Copyright: © 2024 by the authors. Licensee MDPI, Basel, Switzerland. This article is an open access article distributed under the terms and conditions of the Creative Commons Attribution (CC BY) license (https://creativecommons.org/licenses/by/4.0/).

1. Introduction

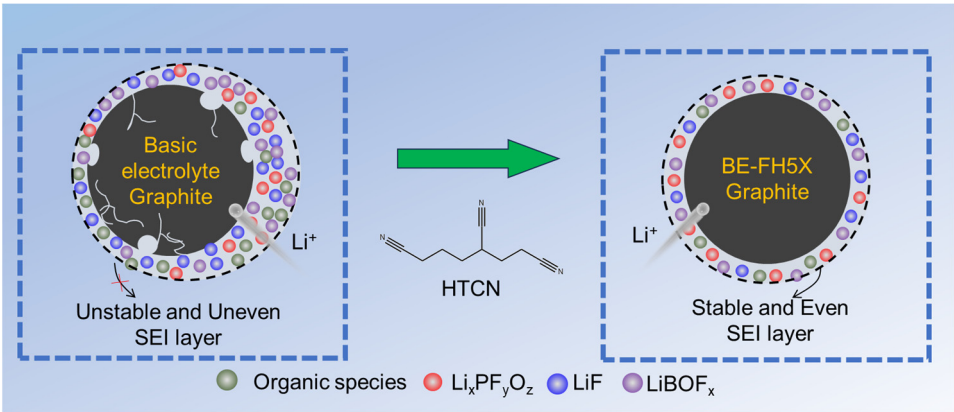
With the rapid development of society, the demand for higher performance lithium-ion batteries (LiBs) has reached unprecedented levels [1,2], driven by the increasing adoption of new energy vehicles [3], portable communication devices [4,5], energy storage stations, etc. [5,6]. Consequently, battery research and application have become prominent topics [7,8]. Over the past decades, electrode-active materials have been recognized as crucial components in LiBs, with extensive research focused on metals and their oxide counterparts as anodes, such as silicon [9,10], cobalt oxide, and iron trioxide [11], due to their high specific theoretical capacity [12,13]. However, despite the advantages, commercial batteries predominantly utilize traditional graphite as the anode material due to its low cost [14,15], wide availability, abundant reserves [16], stable voltage profile, high initial charge–discharge Coulombic efficiency, and stable cycling performance [17–19]. Nevertheless, graphite often suffers from drawbacks during battery cycling, such as the formation of an uneven and unstable solid electrolyte interphase (SEI) layer, leading to the issues like graphite exfoliation, structural degradation, and rapid capacity fade. Consequently, this affects the rate performance and cycling stability of LiBs [20]. Therefore, optimization of

the SEI film formed at the graphite anode during the initial cycles is considered a simple and effective approach to enhance the battery performance [21,22].

The composition of the electrolyte in the LiBs commonly consists of lithium salts and organic carbonates and plays a crucial role in determining the performance of graphite electrodes [23,24]. Upon the initial lithium-ion insertion, a portion of the electrolyte decomposes to form a SEI film [25–27]. This SEI film is thin in thickness, which effectively prevents further electrolyte degradation and preserves the integrity of the graphite electrode, mitigating issues such as exfoliation and cracking [28]. Currently, carbonate-based electrolytes, particularly containing ethylene carbonate (EC), diethyl carbonate (DEC), fluoroethylene carbonate (FEC), dimethyl carbonate (DMC), ethyl methyl carbonate (EMC), etc., are widely used in commercial LiBs, which are also leading the mainstream market of the LiBs. However, during the initial charge/discharge reaction, irreversible capacity decay occurs concurrently with SEI layer formation [29,30]. Moreover, the structure and composition of the SEI layer formed by commercial carbonate electrolytes undergo detrimental changes during extended cycling, leading to increased SEI thickness, impeded Li^+ transfer, and elevated impedance in LiBs. To address these challenges and establish a stable and uniform thin SEI layer on the graphite anode, various additives have been proposed to suppress the decomposition of carbonate electrolytes [31,32].

Fluorine-containing additives, such as FEC molecules, have shown promise in enhancing the properties of the SEI layer when incorporated into conventional electrolytes like $LiPF_6$/EC/DMC electrolytes [33–35]. Quantum chemical calculations have highlighted the role of reduced FEC in promoting the formation of a high-performance SEI layer on the negative electrode surface. However, it should be acknowledged that negligible variability in SEI layer formation has been observed in previous studies [36–38]. Furthermore, the increase in SEI layer thickness during subsequent charge and discharge cycles cannot be overlooked, as it contributes to increased resistance and capacity fade over time. Therefore, understanding and exploring efficient additives to optimize the SEI layer dynamics is crucial for improving LIB performance and longevity [39–42].

In this work, we introduced a precise ratio of FEC and 1,3,6-hexanetrinitrile (HTCN) as dual additives in a 1.0 M $LiPF_6$ electrolyte with EC/DMC (3:7 by volume) to enhance the uniformity and stability of the SEI layer during the initial cycles of LiBs (Scheme 1). Through a series of comprehensive experiments, it was systematically examined that an optimistic FEC/HTCN ratio of 5:4 demonstrated notable advancements in battery cycling performance, capacity retention, and lowered the cell impedance. The reaction mechanism of the LiBs was investigated via ex situ X-ray photo electron spectroscopy (XPS) and scanning electron microscopy (SEM) in detail. With the assistance of HTCN, the formation of an ultrathin and homogeneous SEI film on the graphite anode and increased amount of HTCN would result in a thick SEI layer, while lowering the amount would lead to cracking of SEI at the electrode surface. Our findings underscore the significance of fine-tuning electrolyte composition for optimizing battery performance. By strategically integrating FEC and HTCN additives, we not only achieved enhanced SEI layer uniformity and stability but also mitigated detrimental microstructural changes during battery operation. This approach presents a promising avenue for advancing the development of high-performance lithium-ion batteries with improved efficiency and longevity.



Scheme 1. Schematic illustration of the of the BE-FH5X electrolyte derived SEI on the surface of graphite electrode.

2. Experimental Materials and Methods

2.1. Materials and Agents

An amount of 1.0 M of $LiPF_6$ in EC/DMC (3:7 by volume) solvent with 5.0 wt.% of FEC was purchased from Dodo Chemical Technology Co., Ltd. (Suzhou, China); HTCN was purchased from Aladdin Chemical Reagent Co., Ltd. (Suzhou, China) at ≥98% grade, and used without further purification; polyvinylidene fluoride (PVDF) was purchased from Arkema Co., Ltd. (Paris, France) at ≥99.5% grade; N-methyl pyrrolidone (NMP) was purchased from Sinopharm Chemical Reagent Co., Ltd. (Suzhou, China) at analytical grade; copper foil was bought from Cyber Electrochemical Materials Network Co., Ltd. (Tokyo, Japan) with a thickness of 0.1 mm; commercial graphite powder was purchased from Canrd Materials Co., Ltd. (Guangdong, China).

2.2. Preparation of the Electrolyte

An amount of 1.0 M of $LiPF_6$ in EC/DMC (3:7 by volume) with 5.0 wt.% FEC was adopted as the baseline electrolyte (BE). Afterwards, 0.02 g, 0.04 g, and 0.06 g of HTCN were separately added to sealed aluminum vials containing 1 g of BE electrolyte, and then left to stand at room temperature for 12 h to form the $LiPF_6$-EC/DEC-FEC/HTCN electrolyte systems, denoted as BE-FH52, BE-FH54, and BE-FH56, respectively. The electrolytes were prepared and placed in a highly pure argon-filled glove box with water and oxygen contents of less than 0.1 ppm.

2.3. Preparation of the Graphite Based Electrode

Firstly, 80 mg of commercial graphite powder was placed in an agate mortar and ground for 30 min. Subsequently, 10 mg of PVDF binder and 10 mg of carbon black were added to the mortar and ground for an additional 30 min. After thorough mixing, an appropriate amount of NMP solvent was introduced and the mixture was continuously ground to achieve a homogeneous slurry. This slurry was then coated onto copper foil and dried in a vacuum oven at 80 °C for 8 h. After cooling to room temperature, the active graphite-coated sheet was cut into circular electrodes with a diameter of 13 mm.

2.4. Material Characterization

The morphology and micro-structure of the as-prepared electrodes after 10th cycling in LiBs were characterized by SEM ((Tokyo, Japan), JSM-IT500) equipped with energy dispersive X-ray spectroscopy (EDX, Oxford, UK). X-ray photoelectron spectroscopy (XPS) analysis was performed on the AXIS-ULTRADLD-600W X-ray photoelectron spectrometer (Falconbridge, ON, Canada) to study the evolution of species on the SEI of the electrodes.

2.5. Electrochemical Characterization

LiBs were assembled in an argon glove box with H_2O and O_2 levels below 1 ppm. In detail, the as-prepared graphite circular electrodes were served as cathode and lithium foil as the anode, Celgard 2325 (Canrd Materials Co., Ltd., Guangdong, China) as the separator, and BE-FH as the electrolyte. Discharge/charge performance was performed at a voltage window from 0.001 to 3.00 V using a Neware battery testing system. As for the rate performance test, the charge/discharge rate was as follows: 0.2 C, 0.5 C, 1.0 C, 1.5 C, and 1.0 C for every 5 cycles, and then cycled at 1.0 C for another 15 cycles. Cyclic voltammetry (CV) curves were carried out by applying a multichannel electrochemical workstation (CHI1060, CH instruments, Shanghai, China) between the voltage window of 0.01–3.0 V (vs. Li^+/Li) at a scan rate of 0.1 mV/s. Linear scanning voltammetry (LSV) curves were measured at a voltage window between 0.0 V and 5.5 V (vs. Li^+/Li) at a scanning rate of 5 mV/s. The electrochemical impedances of the batteries were measured on an electrochemical workstation (CHI760E, CH instruments, Shanghai, China). The frequency was set from 1 Hz to 100,000 Hz with the potential amplitude of 5 mV.

3. Results

To study the impact of the BE-FH mixed electrolyte system on the SEI of the graphite anode, a series of tests were conducted. Initially, CV experiments were performed in the range at a voltage window of 0.01–3.0 V to study redox properties of the LiBs with different concentrations of HTCN and FEC additives. Figure 1a illustrates the initial six cycles of CV curves by using BE as the electrolyte. It can be seen that only a reduction current peak and a oxidation peak were observed at potential of approximately 0.02 V and 0.26 V, demonstrating the redox reaction of decomposition of the BE electrolytes to form lithium alkyl carbonate species/lithium insertion into a graphite layer and the desertion of Li^+ from graphite, respectively [43]. Apparently, by adding different percentages of HTCN into the BE, extra reduction and oxidation peaks were observed (Figure 1b–d). According to previous research, the reduction peak at potential of 0.6 V corresponds to the partial decomposition of electrolytes, which results in the formation of the SEI film aiding in the organic component of the SEI film formation—both processes occurring only during the initial cycling period and absent in subsequent cycles [44,45], while the reduction peak at 0.02 V corresponds to the lithium insertion into graphite layer. These results indicate that the formation of the SEI film primarily occurs during the first scan cycle. It is notable that an extra reduction peak at 2.2 V can be shown when increasing the addition of HTCN to 6.0%, which can be explained by the formation of other reduction species on the surface of graphite, which would largely increase the thickness of the SEI, is suspected to inhibit the dynamics of the battery. Comparatively, the BE-FH54-based LiB showed almost overlapped CV curves in subsequent cycles, indicating a highly stable SEI film, which is beneficial to exhibit excellent battery performance, especially cycling stability.

The electrochemical stability of the electrolyte in the working window plays an important role in influencing the overall performance of the battery. Therefore, exploring additives with stable chemical/electrochemical properties is significant. The electrochemical stability of the as-prepared electrolytes was studied via LSV measurements by designing an LiB with bare copper foil at the cathode. As can be seen from Figure 2a, the BE-FH54-based LiB can be stabilized in a very wide voltage range of 1.45–4.30 V compared to BE (1.50–3.15 V), while polarization was more likely to occur outside the voltage window. As anticipated and verified, the presence of mixed additives (FEC+HTCN) sufficiently stabilized against the oxidation of the electrolyte. To investigate cycling performance under different discharge and charge rates, rate performance tests were conducted, which can be seen in Figure 2b. In detail, the capacities of BE-FH54-based LiB at current densities of 0.2 C, 0.5 C, 1.0 C, and 1.5 C were observed to be 328.1 mAh/g, 303.5 mAh/g, 286.3 mAh/g, and 245.6 mAh/g, respectively. The values were significantly higher compared to those of BE-, BE-FH52-, and BE-FH56-based LiB counterparts, which highlighted the crucial role of appropriate amount of the mixed electrolyte additive system (BE-FH54) in regulating

capacities at different rates. Moreover, the rate performance was repeatable, and the capacities showed a negligible change at different rates. It is worth noting that there exists a delicate balance between FEC additives and HTCN additives concerning electrode cycling performance as well as rate performance aspects.

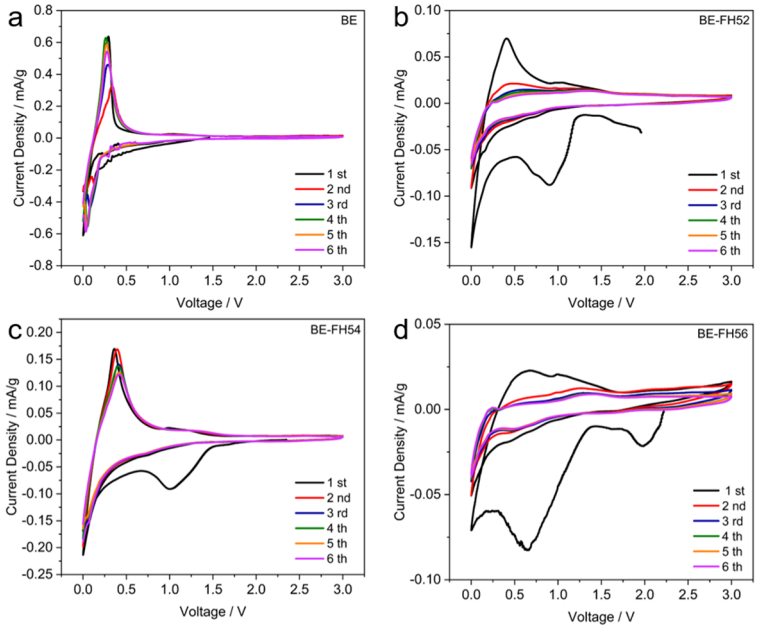


Figure 1. CV curves of the corresponding LiBs with different electrolytes at a voltage window of 0.01–3.0 V (Li/Li^+) by a scan rate of 0.1 mV/s. (**a**) BE, (**b**) BE-FH52, (**c**) BE-FH54, (**d**) BE-FH56.

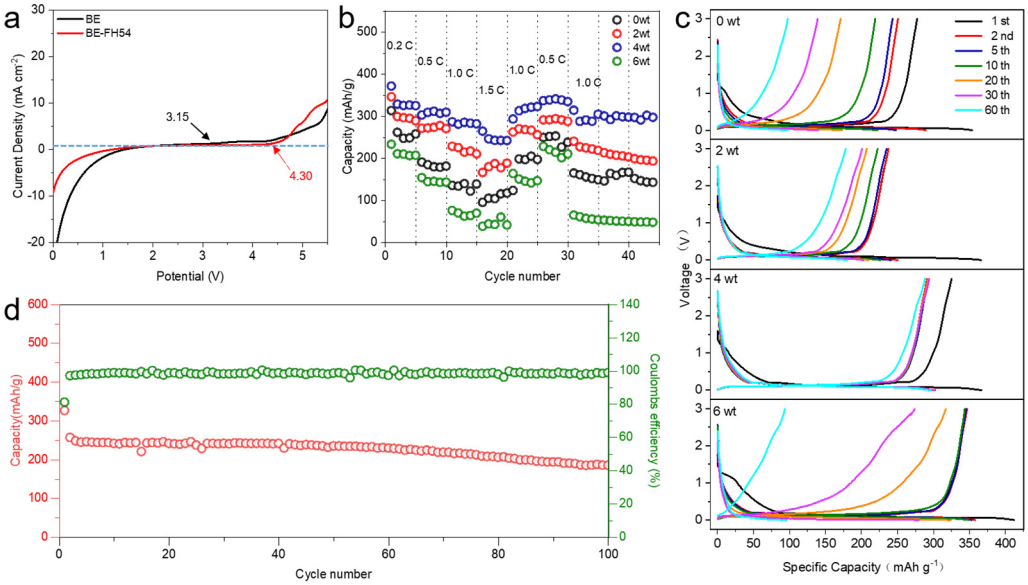


Figure 2. (**a**) LSV curves of BE- and BE-FH54-based LiBs at a scan rate 1 mV/s with a voltage window of 0–5.5 V; (**b**) rate performance of BE-, BE-FH52-, BE-FH54-, and BE-FH56-based LiBs; (**c**) the 1st, 2nd, 10th, 20th, 30th, and 60th discharge/charge curves of BE-, BE-FH52-, BE-FH54-, and BE-FH56-based LiBs; (**d**) cycling stability test of BE-FH54-based LiB at rate of 2.0 C.

Given the exceptional multiplication rate performance exhibited by BE-FH54, its long-term cycling performance emerges as a key parameter with significant implications for practical applications. As shown in Figure 2c, the four LiBs with BE, BE-FH52, BE-FH54, and BE-FH56 electrolytes showed discharge/charge curves at 0.1 C, in which BE-FH56-based LiB demonstrated the highest initial discharge capacity of 411.7 mAh/g (Table 1) with

a first-cycle Coulomb efficiency of 83.9%, but decayed fast with only 92.0 mAh/g left after 60 cycles. The BE-FH54-based LiB showed as initial discharge capacity of 366.7 mAh/g with an initial Coulomb efficiency of 89.0%. The initial capacity was listed at the second place, but the initial Coulomb efficiency value was the highest, demonstrating the synergistic effect of FEC and HTCN in constructing a stable, thin SEI. In addition, the BE-FH54-based LiB maintained discharge and charge capacities of 296.16 mAh/g and 288.1 mAh/g after the 60th cycle, respectively, with an 89.0% capacity retention rate. Comparatively, the BE-FH52 and BE-based LiBs demonstrated a relatively high initial capacity but much inferior Coulomb efficiency and capacity retention. Considering the excellent cycling performance of BE-FH54-based LiB, the cycling performance at higher rates of 2.0 C were conducted. As illustrated in Figure 2d, BE-FH54-based LiB exhibited a stable capacity of ~196 mAh/g over 100 cycles, with a capacity retention rate of 78.4%. The Coulombic efficiency throughout the process remained around 100%, demonstrating the exceptional cycling performance. Therefore, it can be speculated that the BE-FH54 electrolyte positively contributes to the uniformity and stability of the SEI film, thereby enhancing the overall performance of LiBs. Compared to the recent published literature related to organic modified electrolytes in LiBs by applying graphite as the electrode, the capacity of HTCN-FEC-based BE-FH54 LiB takes the top spot (Table S2). It should be noted that the HTCN-FEC features micro-toxicity properties and low costs relative to other listed organic additives, which has potential application in energy storage.

Table 1. Discharge/charge capacities of BE-, BE-FH52-, BE-FH54-, and BE-FH56-based LiBs at 0.1 C.

Sample	IDC	ICC	DC after 60th Cycle	CC after 60th Cycle	ICE	CE after 60th Cycle
BE	353.6 mAh/g	277.3 mAh/g	98.6 mAh/g	96.3 mAh/g	78.4%	97.6%
BE-FH52	366.0 mAh/g	237.6 mAh/g	179.7 mAh/g	177.9 mAh/g	64.9%	98.9%
BE-FH54	366.7 mAh/g	326.4 mAh/g	296.16 mAh/g	288.1 mAh/g	89.0%	97.3%
BE-FH56	411.7 mAh/g	345.4 mAh/g	106.6 mAh/g	104.2 mAh/g	83.8%	97.7%

Note: IDC, ICC, DC, CC, ICE, and CE present the initial discharge capacity, initial charge capacity, discharge capacity, charge capacity, initial Coulombic efficiency, and Coulombic efficiency, respectively.

Despite the battery performance, reaction kinetics are also significant for better understanding the cycling mechanisms of the as-prepared LiBs. On this basis, we delved deeper into the electrochemical kinetics of these electrolyte systems using electrochemical impedance spectroscopy (EIS). As illustrated from the Nyquist plot of Figure 3a, each curve exhibited a distinct diameter of semicircles and oblique straight lines, indicative of different charge transfer and Li^+ diffusion processes. Upon careful fitting by using an equivalent circuit (Figure S1), the diameter of the high-frequency semicircle was found to be directly correlated with the charge transfer resistance (R_{ct}) at the electrode–electrolyte interphase. To quantify these observations, the specific R_{ct} values were extracted and presented in the histograms of Figure 3b. Remarkably, the R_{ct} of the BE-FH54-based LiB (26.79 ohms) was significantly lower compared to BE (77.99 ohms), BE-FH52 (30.17 ohms), and BE-FH56 (31.49 ohms). This conclusion aligns with the electrochemical trends described in Figure 2b,d. Specifically, the Li^+ diffusion rate of BE-FH54 was notably higher than that of other samples, further demonstrating the coordinated regulation of the SEI film by FEC and HTCN additives (Figure 3c,d). It should be noted that the thickness of SEI was in line with the Li^+ diffusion rate. Thus, by applying BE-FH54 as electrolytes, it is speculated that the graphite electrode has a very thin and uniform SEI layer, while increasing or decreasing the proportion of HTCN would cause poor Li^+ diffusion kinetics by forming an inappropriate SEI. These findings not only deepen our understanding of potential electrochemical mechanisms but also underscore the efficacy of customized electrolyte formulations in enhancing battery performance.

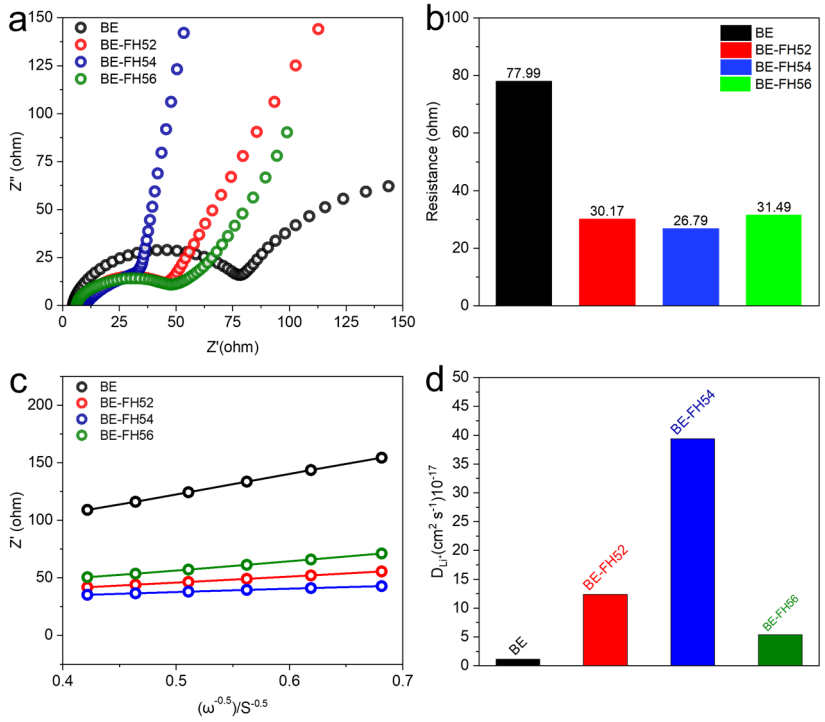


Figure 3. (**a**) Nyquist plots of the fresh assembled cells using BE, BE-FH52, BE-FH54, and BE-FH56 as electrolyte; (**b**) the corresponding histograms of R_{ct} values for different cells; (**c**) Z′ vs. the reciprocal of the square root of frequency ($\omega^{-0.5}$) in the intermediate frequency range for different cells, and (**d**) corresponding histograms of $D_{Li}{}^{+}$.

The surface morphology of the electrodes was characterized by SEM at a discharge/charge rate of 0.1 C for 10 cycles. As shown in Figure 4a, a large number of cracks appeared on the graphite electrode surface of the BE electrolyte-based LiB, indicating the fragile property of the SEI, while the large magnification SEM image (Figure 4b) further confirmed the severe cracks, which adversely affected the cycling performance of the LiBs. The crack showed obvious healing after adding HTCN into the electrolyte (BE-FH52), but small cracks can still be clarified (yellow arrows in Figure 4c,d). The graphite electrode showed a smooth surface and indistinguishable cracks by applying BE-FH54 as the electrolyte (Figure 4e,f), but the surface of the graphite electrode showed a thick coverage of species by further increasing the proportions of HTCN, which may be the main reason of large Li^+ diffusion resistance. Therefore, appropriate HTCN content in the electrolytes is essential to regulate the thickness and mechanical properties of the SEI. Concurrently, the EDX characterization was performed, and corresponding relative atomic percentages of C, O, and F were drawn, as shown in Table S1. As illustrated, the atomic F content gradually decreased with the increasing addition of the HTCN additive, initially demonstrating the existence of HTCN derivatives at the SEI.

To analyze the composition of interfacial layers at the graphite negative electrodes, as well as comprehend their impact on electrochemical performance, XPS spectra of LiBs cycled in different electrolytes were obtained after the fifth cycle, as depicted in Figure 5. In the high-resolution C 1s spectra of Figure 5a, five major peaks were identified. After being fitted according to previous research, the peaks at -CF_2-CH_2 (~290.5 eV) and -CH_2-CF_2 (~285.6 eV) can be attributed to polyvinylidene difluoride (PVDF) binders [46]. And the constituent at ~288.2 eV is assigned to O-C-O/C=O species from the conductivity medium carbon black. The peak at ~284.7 eV is from the C-C/C-H group, while the feature at 284.2 eV can be attributed to the sp^2 hybridized C=C bonds in the FEC. The high-peak intensity of C=C bonds demonstrated that the FEC-derived C=C species was the main composition of SEI. The corresponding bonds were also observed in the fitting spectra of O 1s in Figure 5b at 531 eV (C-O) and 532.5 eV (C=O) [46,47]. Furthermore, it was found that LiB with the BE electrolyte exhibited higher intensities of C-O and C=O peaks

compared to those with the BE-FH electrolyte; and their intensities gradually decreased with the increasing amount of HTCN, indicating that this co-addition of electrolyte can effectively inhibit electrolyte decomposition while improving battery performance. In the F 1s spectra, we observed a significantly stronger presence of LiF (685.5 eV) of the BE-based LiB, indicating that LiF was the main component of the SEI by decomposition of lithium salts and FEC. Upon addition of the hybrid additives of FEC and HTCN, a notable reduction in LiF, $Li_xPO_yF_z$ (≈685.8 eV), and Li_xPF_y(≈687.6 eV) contents with a gradually increasing amount of R-CN species is obvious (Figure 5c,d), demonstrating that the decomposition species from the solvents, FEC, and HTCN formed the main components of SEI for the BE-FH LiBs, and meanwhile, implying that the synergistic effect of FEC and HTCN optimized the SEI at the surface of the graphite electrode. The C≡N in HTCN molecule has a strong coordination ability with Li^+, enabling the formation of stable complexes, which are beneficial to enhance the Li^+ diffusion by forming SEI [48]. Thus, when coupled with the FEC, a high-balanced SEI contributed to the excellent rate performance and cycling stability of the LiBs [48–50].

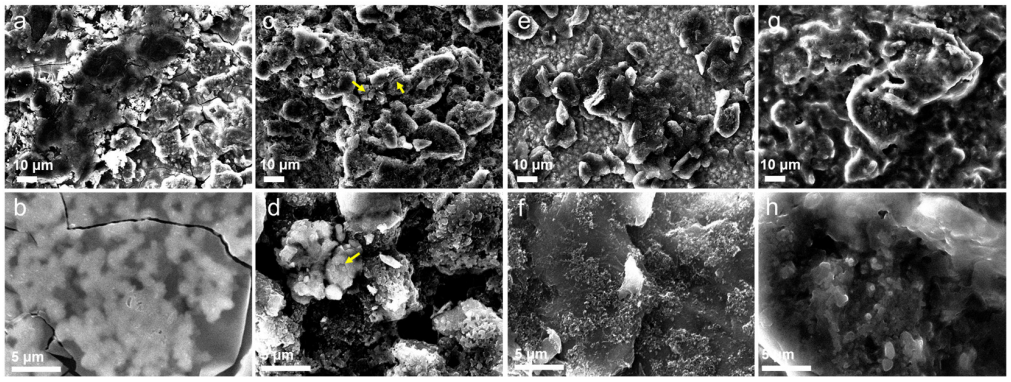


Figure 4. SEM and enlarged magnification SEM images of different LiBs after the 10th cycle. (**a**,**b**) BE; (**c**,**d**) BE-FH52, (**e**,**f**) BE-FH54, and (**g**,**h**) BE-FH56.

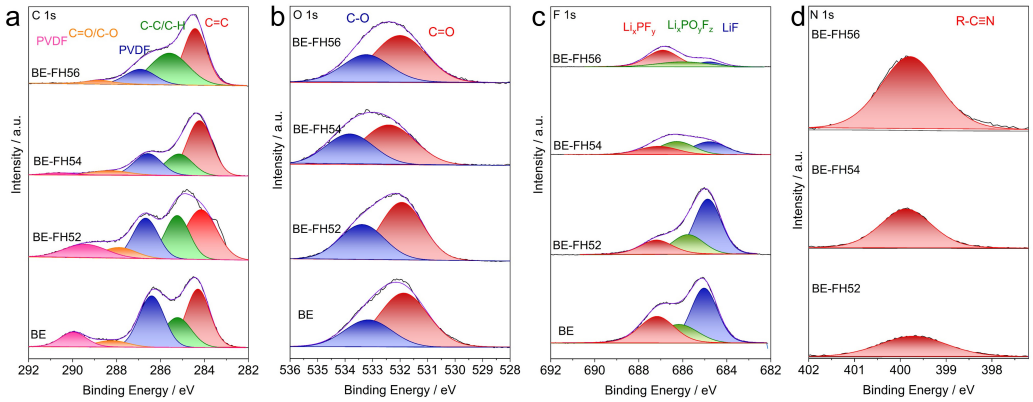


Figure 5. Fitted high-resolution XPS spectrum of graphite electrodes in LiBs after 1st cycle at room temperature. (**a**) C 1s, (**b**) O 1s, (**c**) F 1s and (**d**) N 1s at the BE, BE-FH52, BE-FH54, and BE-FH56.

4. Conclusions

In summary, a series of 1.0 M $LiPF_6$ in EC/DMC (3:7 by volume) electrolytes with different proportions of FEC and HTCN additives were successfully prepared. In terms of the electrochemical measurements, the BE-FH54-based LiB outperformed BE-, BE-FH52-, and BE-FH56-based LiBs with excellent initial Coulombic efficiency (89.0% at 0.1 C), rate performance, and capacity retention (78.4% even at 2.0 C after 100 cycles). The SEM characterization demonstrated the thin and uniform properties of SEI formed by using BE-FH54 as the electrolyte, while the bare BE-based LiB showed obvious cracks at the surface of the electrode. Moreover, the higher or lower the FEC:HTCN proportion resulted

in small cracks and a thick SEI, respectively. The XPS measurements revealed the main components of the SEI for the different BE-FH-based LiBs, and elucidated the synergistic effect of FEC and HTCN, by forming a thin, uniform, and stable SEI assisted with the EIS and SEM results. The research presents methods to enhance battery performance from the electrolyte modification strategy.

Supplementary Materials: The following supporting information can be downloaded at https://www.mdpi.com/article/10.3390/en17133331/s1: Figure S1: Electrical equivalent circuit models for fitting the EIS response of the electrodes and the corresponding equations; Table S1: The relative atomic content of C, O and F at the graphite electrode by applying different electrolytes after 10th cycle; Table S2: Comparison of different additives applied to graphite anode of LiBs on the performance, toxicity/environmental and costs implications. Refs. [51–55] are cited in Supplementary Materials.

Author Contributions: Conceptualization, J.W. and H.L. (Haidong Liu); methodology, H.L. (Hangning Liu); software, H.L. (Hangning Liu); validation, J.W., Y.M., H.L. (Hangning Liu), and Y.C.; formal analysis, J.W.; investigation, H.L. (Hangning Liu), S.W., and L.W.; resources, J.W.; data curation, H.L. (Haidong Liu) and J.W.; writing—original draft preparation, H.L. (Hangning Liu); writing—review and editing, J.W.; visualization, H.L. (Haidong Liu); supervision, J.W. and H.L. (Haidong Liu); project administration, J.W.; funding acquisition, H.L. (Haidong Liu) and J.W. All authors have read and agreed to the published version of the manuscript.

Funding: This research was funded by the China Postdoctoral Science Foundation (2021M701694), Postdoctoral Science Foundation of Jiangsu Province (1006-YBA21038), National Natural Science Foundation of China (22202114), and Experimental Technology Research Project of Qingdao Agricultural University (SYJS202217). This research was also supported by Swedish Energy Agency (P2020-90112 and P2022-00055).

Data Availability Statement: Original data can be obtained from the corresponding authors.

Acknowledgments: The Central Laboratory of Qingdao Agriculture University and Qingdao Engineering Research Center of Agricultural Recycling Economy Materials are acknowledged for the help of physical characterization. We gratefully acknowledge the STandUP for energy for financial support in Sweden.

Conflicts of Interest: The authors declare no conflicts of interest.

References

1. Wang, J.; Guo, X.; Du, X.; Liang, J.; Wu, J.; Zhao, G.; Li, X.; Gui, S.; Zheng, F.; Zhao, J.; et al. Revealing the complex lithiation pathways and kinetics of core-shell NiO@CuO electrode. *Energy Storage Mater.* **2022**, *51*, 11–18. [CrossRef]
2. Li, X.; Liu, S.; Yang, J.; He, Z.; Zheng, J.; Li, Y. Electrochemical methods contribute to the recycling and regeneration path of lithium-ion batteries. *Energy Storage Mater.* **2023**, *55*, 606–630. [CrossRef]
3. Yang, T.; Luo, D.; Zhang, X.; Gao, S.; Gao, R.; Ma, Q.; Park, H.W.; Or, T.; Zhang, Y.; Chen, Z. Sustainable regeneration of spent cathodes for lithium-ion and post-lithium-ion batteries. *Nat. Sustain.* **2024**, *7*, 776–785. [CrossRef]
4. Kim, T.; Song, W.; Son, D.-Y.; Ono, L.K.; Qi, Y. Lithium-ion batteries: Outlook on present, future, and hybridized technologies. *J. Mater. Chem. A* **2019**, *7*, 2942–2964. [CrossRef]
5. Deng, R.; He, T. Flexible Solid-State Lithium-Ion Batteries: Materials and Structures. *Energies* **2023**, *16*, 4549. [CrossRef]
6. Zuo, W.; Luo, M.; Liu, X.; Wu, J.; Liu, H.; Li, J.; Winter, M.; Fu, R.; Yang, W.; Yang, Y. Li-rich cathodes for rechargeable Li-based batteries: Reaction mechanisms and advanced characterization techniques. *Energy Environ. Sci.* **2020**, *13*, 4450–4497. [CrossRef]
7. Chen, Z.; Chao, Y.; Li, W.; Wallace, G.G.; Bussell, T.; Ding, J.; Wang, C. Abuse-Tolerant Electrolytes for Lithium-Ion Batteries. *Adv. Sci.* **2021**, *8*, 2003694. [CrossRef]
8. Logan, E.R.; Dahn, J.R. Electrolyte Design for Fast-Charging Li-Ion Batteries. *Trends Chem.* **2020**, *2*, 354–366. [CrossRef]
9. Guo, J.; Zhao, G.; Xie, T.; Dong, D.; Ma, C.; Su, L.; Gong, L.; Lou, X.; Guo, X.; Wang, J.; et al. Carbon/Polymer Bilayer-Coated Si-SiOx Electrodes with Enhanced Electrical Conductivity and Structural Stability. *ACS Appl. Mater. Interfaces* **2020**, *12*, 19023–19032. [CrossRef]
10. Sun, Z.; Yin, Q.; Chen, H.; Li, M.; Zhou, S.; Wen, S.; Pan, J.; Zheng, Q.; Jiang, B.; Liu, H.; et al. Building better solid-state batteries with silicon-based anodes. *Interdiscip. Mater.* **2023**, *2*, 635–663. [CrossRef]
11. Xie, T.; Liu, H.; Wang, L.; Wang, J.; Ma, C.; Xuan, C.; Su, L.; Gong, L. Rational Regulation of Cu-Co Thiospinel Hierarchical Microsphere to Enhance the Supercapacitive Properties. *Batter. Supercaps* **2023**, *6*, e202300317. [CrossRef]

12. Sammawipawekul, N.; Kaeosamut, N.; Autthawong, T.; Watwiangkham, A.; Suthirakun, S.; Wannapaiboon, S.; Mahamai, N.; Sarakonsri, T.; Chimupala, Y.; Yimklan, S. Isostructural dual-ligand-based MOFs with different metal centers in response to diverse capacity lithium-ion battery anode. *Chem. Eng. J.* **2024**, *482*, 148904. [CrossRef]
13. Chen, Y.; Yang, J.; He, A.; Li, J.; Ma, W.; Record, M.-C.; Boulet, P.; Wang, J.; Albina, J.-M. Core–Double-Shell TiO_2@Fe_3O_4@C Microspheres with Enhanced Cycling Performance as Anode Materials for Lithium-Ion Batteries. *Materials* **2024**, *17*, 2543. [CrossRef]
14. Sung, J.H.; Kim, T.; Kim, S.; Hasan, F.; Mohanty, S.K.; Srinivasa, M.K.; Reddy, S.C.; Yoo, H.D. Li_3PO_4-Coated Graphite Anode for Thermo-Electrochemically Stable Lithium-Ion Batteries. *Energies* **2023**, *16*, 6141. [CrossRef]
15. Wen, Y.; Liu, H.; Jiang, X. Preparation of graphite anode slurry by one-pot method. *J. Energy Storage* **2023**, *73*, 108973. [CrossRef]
16. Zhang, H.; Song, Z.; Fang, J.; Li, K.; Zhang, M.; Li, Z.; Yang, L.; Pan, F. Electrolyte Optimization for Graphite Anodes toward Fast Charging. *J. Phys. Chem. C* **2023**, *127*, 2755–2765. [CrossRef]
17. Min, W.; Chen, X.; Huang, S.; Liao, Y.; Liang, Z.; Lei, Y.; Xu, J. High performance lithium ion battery cathode based reduced holey graphene oxides from spent lithium ion batteries. *Carbon* **2023**, *210*, 118038. [CrossRef]
18. Xu, J.; Wang, X.; Hu, B.; Ding, J.; Zhang, Z.; Ge, S. Oriented-Etched Graphite for Low-Temperature Lithium-Ion Batteries. *Batter. Supercaps* **2023**, *6*, e202200499. [CrossRef]
19. Lochala, J.A.; Zhang, H.; Wang, Y.; Okolo, O.; Li, X.; Xiao, J. Practical Challenges in Employing Graphene for Lithium-Ion Batteries and Beyond. *Small Methods* **2017**, *1*, 1700099. [CrossRef]
20. Krajewski, M.; Chen, C.-H.; Huang, Z.-T.; Lin, J.-Y. $Li_4Ti_5O_{12}$ Coated by Biomass-Derived Carbon Quantum Dots as Anode Material with Enhanced Electrochemical Performance for Lithium-Ion Batteries. *Energies* **2022**, *15*, 7715. [CrossRef]
21. Yang, Y.; Yang, W.; Yang, H.; Zhou, H. Electrolyte design principles for low-temperature lithium-ion batteries. *eScience* **2023**, *3*, 100170. [CrossRef]
22. Sun, L.; Wang, Y.; Kong, L.; Chen, S.; Peng, C.; Zheng, J.; Li, Y.; Feng, W. Designing mesostructured iron (II) fluorides with a stable in situ polymer electrolyte interface for high-energy-density lithium-ion batteries. *eScience* **2024**, *4*, 100188. [CrossRef]
23. Kotronia, A.; Asfaw, H.D.; Tai, C.-W.; Hahlin, M.; Brandell, D.; Edström, K. Nature of the Cathode–Electrolyte Interface in Highly Concentrated Electrolytes Used in Graphite Dual-Ion Batteries. *ACS Appl. Mater. Interfaces* **2021**, *13*, 3867–3880. [CrossRef]
24. Domi, Y.; Doi, T.; Tsubouchi, S.; Yamanaka, T.; Abe, T.; Ogumi, Z. Irreversible morphological changes of a graphite negative-electrode at high potentials in LiPF6-based electrolyte solution. *Phys. Chem. Chem. Phys.* **2016**, *18*, 22426–22433. [CrossRef] [PubMed]
25. Yang, G.; Zhang, S.; Weng, S.; Li, X.; Wang, X.; Wang, Z.; Chen, L. Anionic Effect on Enhancing the Stability of a Solid Electrolyte Interphase Film for Lithium Deposition on Graphite. *Nano Lett.* **2021**, *21*, 5316–5323. [CrossRef] [PubMed]
26. Wang, M.; Peng, Z.; Luo, W.; Ren, F.; Li, Z.; Zhang, Q.; He, H.; Ouyang, C.; Wang, D. Tailoring Lithium Deposition via an SEI-Functionalized Membrane Derived from LiF Decorated Layered Carbon Structure. *Adv. Energy Mater.* **2019**, *9*, 1802912. [CrossRef]
27. Zheng, X.; Shi, Q.; Wang, Y.; Battaglia, V.S.; Huang, Y.; Zheng, H. The role of carbon bond types on the formation of solid electrolyte interphase on graphite surfaces. *Carbon* **2019**, *148*, 105–114. [CrossRef]
28. Parhizi, M.; Caceres-Martinez, L.E.; Modereger, B.A.; Kenttämaa, H.I.; Kilaz, G.; Ostanek, J.K. Determining the Composition of Carbonate Solvent Systems Used in Lithium-Ion Batteries without Salt Removal. *Energies* **2022**, *15*, 2805. [CrossRef]
29. Pang, C.; Xu, G.; An, W.; Ding, G.; Liu, X.; Chai, J.; Ma, J.; Liu, H.; Cui, G. Three-Component Functional Additive in a LiPF6-Based Carbonate Electrolyte for a High-Voltage $LiCoO_2$/Graphite Battery System. *Energy Technol.* **2017**, *5*, 1979–1989. [CrossRef]
30. Xie, J.-D.; Patra, J.; Chandra Rath, P.; Liu, W.-J.; Su, C.-Y.; Lee, S.-W.; Tseng, C.-J.; Gandomi, Y.A.; Chang, J.-K. Highly concentrated carbonate electrolyte for Li-ion batteries with lithium metal and graphite anodes. *J. Power Source* **2020**, *450*, 227657. [CrossRef]
31. Zhou, M.; Fan, Y.; Gao, Y.; Ma, Z.; Liu, Z.; Wang, W.; Younus, H.A.; Chen, Z.; Wang, X.; Zhang, S. Less is More: Trace Amount of a Cyclic Sulfate Electrolyte Additive Enable Ultra-Stable Graphite Anode for High-Performance Potassium-Ion Batteries. *ACS Appl. Mater. Interfaces* **2022**, *14*, 44429–44438. [CrossRef] [PubMed]
32. Lei, Q.; Yang, T.; Zhao, X.; Fan, W.; Wang, W.; Yu, L.; Guo, S.; Zuo, X.; Zeng, R.; Nan, J. Lithium difluorophosphate as a multi-functional electrolyte additive for 4.4V $LiNi_{0.5}Co_{0.2}Mn_{0.3}O_2$/graphite lithium ion batteries. *J. Electroanal. Chem.* **2019**, *846*, 113141. [CrossRef]
33. Ma, C.; Qiu, Z.; Shan, B.; Song, Y.; Zheng, R.; Feng, W.; Cui, Y.; Xing, W. The optimization of the electrolyte for low temperature $LiFePO_4$-graphite battery. *Mater. Lett.* **2024**, *356*, 135594. [CrossRef]
34. Uchida, S.; Ishikawa, M. Lithium bis(fluorosulfonyl)imide based low ethylene carbonate content electrolyte with unusual solvation state. *J. Power Source* **2017**, *359*, 480–486. [CrossRef]
35. Guan, D.; Hu, G.; Peng, Z.; Cao, Y.; Wu, J.; Huang, M.; Zhang, S.; Dai, Y.; Gong, Y.; Du, K. A nonflammable low-concentration electrolyte for lithium-ion batteries. *J. Mater. Chem. A* **2022**, *10*, 12575–12587. [CrossRef]
36. Liu, Z.; Li, R.; Deng, T. Optimized electrolyte design for improved mechanical stability of NCM523/Gr batteries at 4.6V cycles. *J. Mater. Res.* **2023**, *38*, 4795–4804. [CrossRef]
37. Wu, Y.; Zhang, W.; Li, Y.; Feng, X.; Ma, Z.; Ren, D.; Lu, L.; Xu, G.-L.; Amine, K.; Ouyang, M. Solid-state interphases design for high-safety, high-voltage and long-cyclability practical batteries via ethylene carbonate-free electrolytes. *Energy Storage Mater.* **2024**, *65*, 103165. [CrossRef]

38. Hu, Y.-S.; Lu, Y. The Mystery of Electrolyte Concentration: From Superhigh to Ultralow. *ACS Energy Lett.* **2020**, *5*, 3633–3636. [CrossRef]
39. Liu, D.; Qian, K.; He, Y.-B.; Luo, D.; Li, H.; Wu, M.; Kang, F.; Li, B. Positive film-forming effect of fluoroethylene carbonate (FEC) on high-voltage cycling with three-electrode $LiCoO_2$/Graphite pouch cell. *Electrochim. Acta* **2018**, *269*, 378–387. [CrossRef]
40. He, M.; Su, C.-C.; Feng, Z.; Zeng, L.; Wu, T.; Bedzyk, M.J.; Fenter, P.; Wang, Y.; Zhang, Z. High Voltage $LiNi_{0.5}Mn_{0.3}Co_{0.2}O_2$/Graphite Cell Cycled at 4.6 V with a FEC/HFDEC-Based Electrolyte. *Adv. Energy Mater.* **2017**, *7*, 1700109. [CrossRef]
41. Kang, S.; Geng, F.; Lou, X.; Lu, G.; Liao, Y.; Shen, M.; Hu, B. Understanding the Improved Fast Charging Performance of Graphite Anodes with a Fluoroethylene Carbonate Additive by In Situ NMR and EPR. *ACS Appl. Energy Mater.* **2023**, *6*, 7596–7606. [CrossRef]
42. Ehteshami, N.; Ibing, L.; Stolz, L.; Winter, M.; Paillard, E. Ethylene carbonate-free electrolytes for Li-ion battery: Study of the solid electrolyte interphases formed on graphite anodes. *J. Power Source* **2020**, *451*, 227804. [CrossRef]
43. Sasanka Hewathilake, H.P.T.; Karunarathne, N.; Wijayasinghe, A.; Balasooriya, N.W.B.; Arof, A.K. Performance of developed natural vein graphite as the anode material of rechargeable lithium ion batteries. *Ionics* **2017**, *23*, 1417–1422. [CrossRef]
44. Kasnatscheew, J.; Wagner, R.; Winter, M. Fluoroethylene Carbonate As an Promising Additive for γ-Butyrolactone based Electrolytes. *ECS Meet. Abstr.* **2014**, *MA2014-01*, 37.
45. Farhat, D.; Maibach, J.; Eriksson, H.; Edström, K.; Lemordant, D.; Ghamouss, F. Towards high-voltage Li-ion batteries: Reversible cycling of graphite anodes and Li-ion batteries in adiponitrile-based electrolytes. *Electrochim. Acta* **2018**, *281*, 299–311. [CrossRef]
46. Liu, H.; Naylor, A.J.; Menon, A.S.; Brant, W.R.; Edström, K.; Younesi, R. Understanding the Roles of Tris(trimethylsilyl) Phosphite (TMSPi) in $LiNi_{0.8}Mn_{0.1}Co_{0.1}O_2$ (NMC811)/Silicon–Graphite (Si–Gr) Lithium-Ion Batteries. *Adv. Mater. Interfaces* **2020**, *7*, 2000277. [CrossRef]
47. Younesi, R.; Christiansen, A.S.; Scipioni, R.; Ngo, D.-T.; Simonsen, S.B.; Edström, K.; Hjelm, J.; Norby, P. Analysis of the Interphase on Carbon Black Formed in High Voltage Batteries. *J. Electrochem. Soc.* **2015**, *162*, A1289. [CrossRef]
48. Tang, C.; Chen, Y.; Zhang, Z.; Li, W.; Jian, J.; Jie, Y.; Huang, F.; Han, Y.; Li, W.; Ai, F.; et al. Stable cycling of practical high-voltage $LiCoO_2$ pouch cell via electrolyte modification. *Nano Res.* **2023**, *16*, 3864–3871. [CrossRef]
49. Kim, S.; Lee, J.-A.; Lee, D.G.; Son, J.; Bae, T.H.; Lee, T.K.; Choi, N.-S. Designing Electrolytes for Stable Operation of High-Voltage $LiCoO_2$ in Lithium-Ion Batteries. *ACS Energy Lett.* **2024**, *9*, 262–270. [CrossRef]
50. Li, X.; Han, X.; Li, G.; Du, J.; Cao, Y.; Gong, H.; Wang, H.; Zhang, Y.; Liu, S.; Zhang, B.; et al. Nonsacrificial Nitrile Additive for Armoring High-Voltage $LiNi_{0.83}Co_{0.07}Mn_{0.1}O_2$ Cathode with Reliable Electrode–Electrolyte Interface toward Durable Battery. *Small* **2022**, *18*, 2202989. [CrossRef]
51. Huang, L.; Chen, S.; Zhan, J.; Liang, J.; Li, S.; Wang, H.; Xu, M.; Li, W. Insight into the role of fluoroethylene carbonate in solid electrolyte interphase construction for graphite anodes of lithium-ion batteries. *J. Phys. Chem. C* **2024**, *128*, 9586–9594. [CrossRef]
52. Zhou, K.; Yang, H.; Zhou, J.; Tian, Y.; Guo, J.; Yuan, M.; Liu, L.; Gai, L. Abnormal electrode behavior of graphite anode operating with the electrolyte containing vinylene carbonate and ethylene sulfite additives. *Electrochim. Acta* **2023**, *462*, 142768. [CrossRef]
53. Qiu, Y.; Lu, D.; Gai, Y.; Cai, Y. Adiponitrile (ADN): A Stabilizer for the $LiNi_{0.8}Co_{0.1}Mn_{0.1}O_2$ (NCM811) electrode/electrolyte interface of a graphite/NCM811 Li-ion cell. *ACS Appl. Mater. Interfaces* **2022**, *14*, 11398–11407.
54. Wen, F.; Cao, S.; Ren, X.; Cao, Y.; Ai, X.; Xu, F. Nonflammable dual-salt electrolytes for graphite/$LiNi_{0.8}Co_{0.1}Mn_{0.1}O_2$ lithium-ion batteries: Li^+ solvation structure and electrode/eelectrolyte interphase. *ACS Appl. Energy Mater.* **2022**, *5*, 15491–15501. [CrossRef]
55. Lu, D.; He, J.; Qiu, Y.; Zhu, J.; Zhang, M.; Cai, Y. Using triallyl phosphate as electrolyte additive to stabilize electrode–electrolyte interface of $LiNi_{0.5}Mn_{1.5}O_4$/graphite high voltage lithium ion cells. *ACS Appl. Energy Mater.* **2022**, *5*, 13600–13609. [CrossRef]

Disclaimer/Publisher's Note: The statements, opinions and data contained in all publications are solely those of the individual author(s) and contributor(s) and not of MDPI and/or the editor(s). MDPI and/or the editor(s) disclaim responsibility for any injury to people or property resulting from any ideas, methods, instructions or products referred to in the content.